IDA

INSTITUTE FOR DEFENSE ANALYSES

Antenna Effects on Polarimetric Imagery in Ultrawide Synthetic Aperture Radar

James M. Ralston
Elizabeth Li Ayers

September 2002

Approved for public release;
distribution unlimited.

IDA Document D-2735

Log: H 02-001382

This work was conducted under contract DASW01 98 C 0067, Task DA-2-155, for DARPA/IXO. The publication of this IDA document does not indicate endorsement by the Department of Defense, nor should the contents be construed as reflecting the official position of that Agency.

© 2002, 2003 Institute for Defense Analyses, 4850 Mark Center Drive, Alexandria, Virginia 22311-1882 • (703) 845-2000.

This material may be reproduced by or for the U.S. Government pursuant to the copyright license under the clause at DFARS 252.227-7013 (NOV 95).

INSTITUTE FOR DEFENSE ANALYSES

IDA Document D-2735

Antenna Effects on Polarimetric Imagery in Ultrawide Synthetic Aperture Radar

James M. Ralston
Elizabeth Li Ayers

PREFACE

This document was prepared for the Information Exploitation Office of the Defense Advanced Research Projects Agency. The work reported was accomplished for the DARPA program on Countering Camouflage, Concealment and Deception (CCCD).

CONTENTS

FIGURES

ANTENNA EFFECTS ON POLARIMETRIC IMAGERY IN ULTRAWIDE SYNTHETIC APERTURE RADAR

1. INTRODUCTION

The value of collecting and processing fully polarimetric data in synthetic aperture radar (SAR) has been firmly established (Refs. 1, 2, 3). Polarimetric decomposition of SAR data at low resolution has led to the development of techniques for automatic terrain and scene classification (Refs. 2, 3), and polarimetric processing at higher resolution has been shown not only to reduce scene radiometric noise but also to support improved classification of individual targets (Refs. 1, 4). For the most part, these benefits have been demonstrated at SAR frequencies in the upper microwave bands, where high resolutions in both range and cross range are obtained with relatively small SAR integration angles (~3 deg) and signal waveform percentage bandwidths (<10 percent).

Because of these successes, many of the developers of ultrawide SARs, which operate in the VHF and UHF spectral bands, are investigating the application of similar polarimetric methods. Typical ultrawide SARs, however, operate over angular beamwidths of up to 90 deg or more, and the bandwidth-to-center-frequency ratio can exceed 100 percent. Moreover, practical considerations of platform integration generally lead to physical constraints on antenna design that inevitably affect electromagnetic performance. Consequently, the instantaneous wave polarization received at a single point to be imaged will vary significantly over these wide frequency and angular apertures, not only due to inherent and unavoidable deviations in geometrical projection (which are not the subject of this paper), but also as a result of inevitable discrepancies between the nominal, intended wave polarization and the polarization realized by a practical antenna in a given direction. These antenna effects could have serious implications for the accuracy and interpretation of ultrawide polarimetric SAR imagery. To gauge the impact of practical antenna cross polarization we have exploited an exhaustively thorough set of measurements on an existing antenna prototype intended to support ultrawide polarimetric SAR in the VHF and UHF bands (150–550 MHz).

2. ANTENNA DESCRIPTION

The antenna prototype developed by Ball Aerospace (Ref. 5) consists of an array of circular electrodes on a polyhedral surface over a resonant cavity. In Figure 1, this antenna is shown inverted. The size and shape of this prototype are driven by the need to fit into the available volume of an unmanned aerial vehicle (UAV), in this case the Global Hawk. This packaging requirement has forced notable departures from the desirable symmetry characteristics that normally support good cross-polarized response. The radiating elements of this array are the points of tangency between the circular elements. This array is configured so that either the vertical or horizontal points of tangency can be fed using a balanced transmission line with the intent of providing linearly polarized radiation in either the vertical or horizontal planes. Figure 1 illustrates the case in which the horizontal points are fed. This feed condition is denoted "H-Port." Feeding the vertical points of tangency is denoted "V-Port."

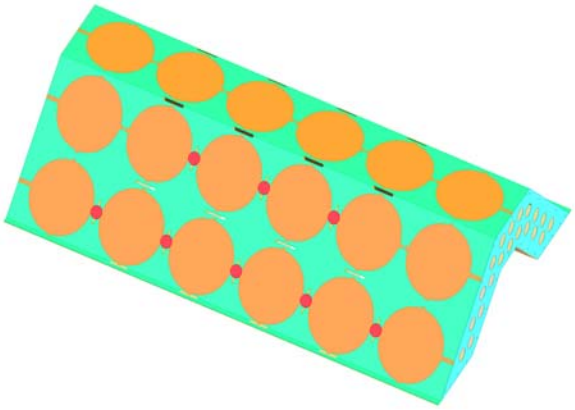

Figure 1. UHF Circles Array Fabricated by Ball Aerospace, Shown Inverted from Normal Orientation. This view illustrates the feed points for achieving nominal horizontal polarization.

Depending on the particular elements chosen for excitation and their phasing, the beam is principally directed to either the left or right sides of the platform aircraft at a nominal depression angle of 30 deg below horizontal. Other than this, there is no attempt to steer the beam electronically. Because the antenna is required to operate over a very wide bandwidth, it is inevitably electrically small at the lowest frequency, so that pattern directionality is difficult to maintain, as well as polarization purity at the angle extremes of the synthetic aperture.

For this program, Ball Aerospace constructed both full-scale and 1/4-scale models. The data set exploited in this paper was measured on the 1/4-scale model in a scaled fuselage model of the Global Hawk aircraft. Ball Aerospace made all

measurements of the 1/4-scale article over the 600–2,200 MHz band, equivalent to 150–550 MHz full scale. Pattern measurements for all antennas were made over a full 4π steradians. At each point in angle-frequency space, antenna response was measured with respect to two orthogonal, linearly polarized sources. All measurements were fully coherent with respect to frequency and polarization. Thus, the data can be used to synthesize the antenna's response to any arbitrary polarization. In the case studied here, we will use the true polarization of the transmitted signal together with the true polarimetric response to synthesize the apparent polarimetric signature of "pure" targets in a known polarimetric basis.

3. ANTENNA MEASUREMENTS

Figure 2 shows the coordinate system. At each value of (scaled) frequency from 150 to 550 MHz, antenna pattern measurements in orthogonal linear polarizations corresponding to the θ (horizontal) and ϕ (vertical) directions were made over the full 4π radiation sphere. Note that in this coordinate system, lines of constant ϕ correspond to SAR Integration path at depression angle ϕ and that θ is the angular integration variable. As the SAR overflies a point on the ground, the illumination polarization varies from the nominal desired polarization. This point is illustrated for nominal horizontal polarization in Figure 3, which plots the trajectory of measured polarization on the Poincaré sphere (depicted as a flat surface) as θ varies from 45 to 135 deg at a depression angle of –30 deg. The ellipse shows the boundary of points for which the undesired polarization component is at least 15 dB below the desired polarization. For emphasis, Figure 3 shows the most dramatic departure from ideal polarization. Figure 4 represents another case for which the off-polarization component is generally within the –15 dB region. Not surprisingly, the lowest frequencies exhibited the largest departures from nominal polarization.

The Poincaré sphere is well known and widely used as a medium for displaying wave polarization, but it does not readily lend itself to scattering calculations. For this we convert the complex phasor field measurements, $\boldsymbol{E_{Xh}}$ and $\boldsymbol{E_{Xv}}$ (where X stands for either H or V, the nominal horizontal or vertical antenna port, and the lower case v or h denote the true field polarizations), in the orthogonal linear basis to complex spatial vectors (Ref. 6):

$$\overline{E}_X = E_{Xh} \cdot \hat{i} + E_{Xv} \cdot \hat{j} \quad . \tag{1}$$

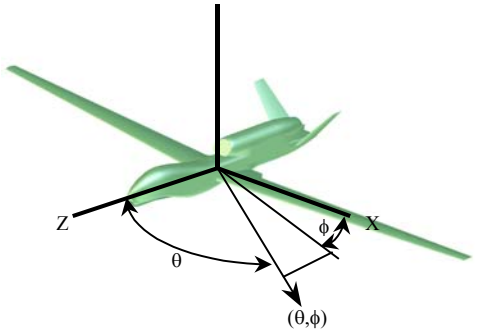

Figure 2. The Aircraft Spherical Coordinate System (ASCS) Defined for the Ball Antenna Analyses. Note that the polar angle, θ, is measured with respect to the aircraft nose, and the nominal "azimuthal" angle, ϕ, is measured in the roll-plane.

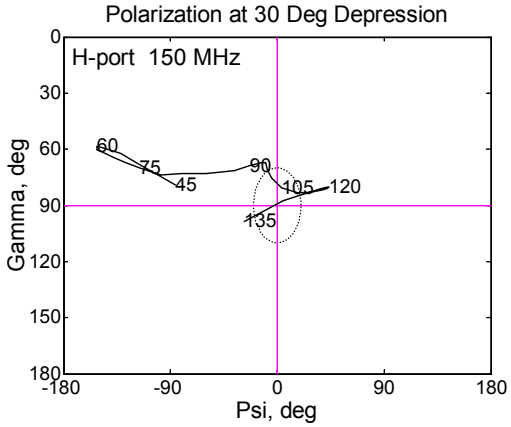

Figure 3. Polarization Purity of 1/4-scale Antenna. The coordinates (psi, gamma) are the Poincaré sphere plotted as a plane. The point psi = 0, gamma = 90 deg represents perfect horizontal polarization. The polarization trajectory is shown over a 90-deg azimuth beam width centered at broadside and at a 30-deg depression angle. Polarization points within the dotted region correspond to at least 15 dB of cross-polarized rejection.

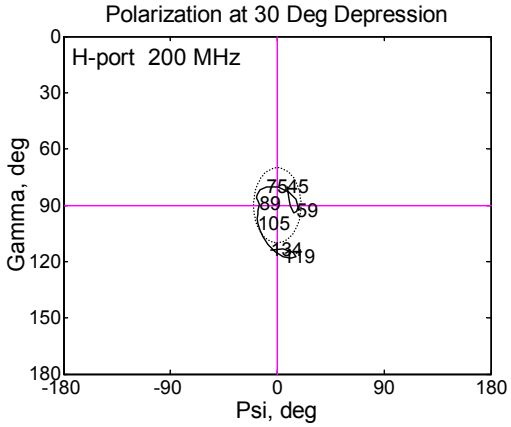

Figure 4. Same as Figure 3, but at a Slightly Higher Frequency. Note that in this case the polarization trajectory remains almost entirely within the goal region.

This complex vector is reduced to a unit complex vector corresponding to each port of the antenna:

$$\hat{e}_X = \overline{E}_X \Big/ \left|\overline{E}_X\right| \quad . \tag{2}$$

From these complex vectors we can form a complex (2 × 2) matrix describing the antenna response to a wave of arbitrary polarization:

$$\mathrm{A} = \begin{pmatrix} \hat{e}_{Hh} & \hat{e}_{Hv} \\ \hat{e}_{Vh} & \hat{e}_{Vv} \end{pmatrix} \quad . \tag{3}$$

This matrix is a function of frequency as well as direction (θ, ϕ). The off-diagonal elements of A give an immediate indication of polarization quality. The magnitudes of these elements are plotted in Figures 5 and 6 at a 30-deg grazing angle for the nominal H and V antenna ports, respectively. Note that although cross-polarized response deteriorates at large off-boresight angles, there is a broad region of ±30 deg from broadside for which cross-polarized isolation is generally 15 dB or better. It is this region of response that we hope to exploit in SAR polarimetry.

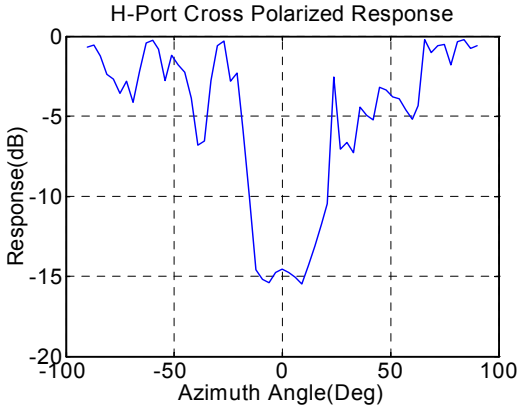

Figure 5. Cross-Polarized Response of H Antenna Port. The curve represents the envelope of the maximum response at each frequency from 200 to 550 MHz. Note the valley of good cross polarization occurring near broadside (0 deg).

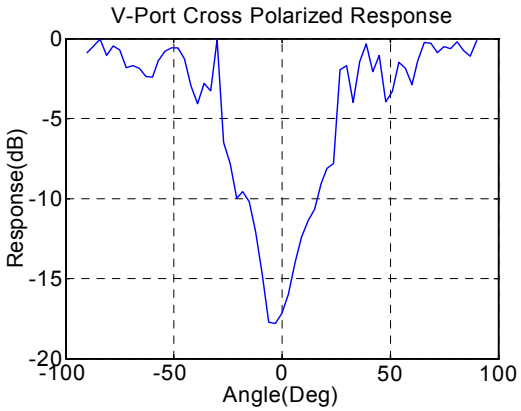

Figure 6. Cross-Polarized Response of V Antenna Port as for Figure 5. Note here as well that cross-polarized response is acceptably low near broadside.

4. CANONICAL SCATTERERS

The goal of SAR polarimetry is to exploit the scattering matrices that may be unique to specific scatterers or scattering regions in order to (1) classify targets or terrain types or (2) separate ground-level scattering from that originating in elevated foliage (Ref. 7). To gauge the impact of imperfections in antenna polarimetric response, we define a canonical linear-polarization basis set of scattering matrices corresponding to sphere-like (odd-bounce, trihedral, etc.) targets, 0-deg diplanes, and 45-deg diplanes. The polarization directions of the scatterers are defined to be the same as those used in the antenna measurements. Thus:

$$S_{sphere} = \begin{pmatrix} -1 & 0 \\ 0 & -1 \end{pmatrix}$$

$$S_{d00} = \begin{pmatrix} 1 & 0 \\ 0 & -1 \end{pmatrix} \quad . \tag{4}$$

$$S_{d45} = \begin{pmatrix} 0 & 1 \\ 1 & 0 \end{pmatrix}$$

These matrices are sufficient to represent the polarimetric response of any discrete target. The measured backscatter from one of these targets, S_{meas}, will differ from its ideal scatter matrix due to antenna cross-polarization effects. The ideal and measured scattering matrices are related to the antenna characteristics by (Ref. 6):

$$S_{meas} = A \cdot S_{ideal} \cdot A^T \quad , \tag{5}$$

where A^T is the transpose of the antenna matrix, A. So defined, S_{meas} depends on θ, ϕ, and f through A. The effect of SAR imaging over a finite aperture is obtained by integrating Equation (5) over angle and frequency to obtain *S*:

$$S = \iint_{\theta, f} S_{meas} \cdot W(\theta, f) d\theta df \quad . \tag{6}$$

Here, *W* represents a weighting function that accounts for: the f^2 antenna gain variation with frequency, $1/R^4$ energy collection taper over the synthetic aperture, non-uniform angular sampling density over the synthetic aperture, and a two-dimensional Hann window. The antenna matrix, A, is obtained from direct physical measurements and includes non-ideal amplitude and phase variations in each polarization component. These subtle variations in antenna response are not reflected in the weight matrix, W. As a result, W does not represent an ideal matched filter to the synthesized polarization responses, S_{meas}. The resulting mismatch losses, although small, will be evident in the polarization decomposition performed below. In the examples that follow, we have taken

an integration aperture from 150–550 MHz and ±30 deg from broadside. Note that the matrix S still retains a dependence on the antenna depression angle, ϕ.

5. SCATTER MATRIX DECOMPOSITION

For backscattering from reciprocal targets, the integrated scatter matrix, S, is readily placed in the form

$$S = \begin{pmatrix} a+b & c \\ c & a-b \end{pmatrix} \quad , \tag{7}$$

from which the (generally complex) parameters a, b, and c are easily related to the scattering strength of canonical scatterers in the chosen basis (Equation 4). If the antenna polarization characteristics were ideal over the synthetic aperture, A would be the identity matrix, and the resulting S matrix would be identical to the original canonical matrix. For the practical antenna, the decompositions of backscatter from ideal targets are shown in Figures 7 through 9. Note that because of the mismatch between the synthesized antenna port response and the weight matrix, W, the sum of the powers projected into the three canonical scatterers is not exactly unity.

The discrepancy, or mismatch loss, is plotted in Figure 10. The best polarimetric performance, as indicated by the degree of projection of the measured scatterer on the originating component, tends to occur at the steeper grazing angles. At shallower grazing angles the apparent asymmetry of the antenna, as viewed from the target, is much greater, leading to somewhat degraded polarimetric purity. The design point of this antenna was a 30-deg grazing angle; at this grazing angle the polarimetric fidelity is greater than 80 percent. Note also that the mismatch losses are minimum near this same grazing angle.

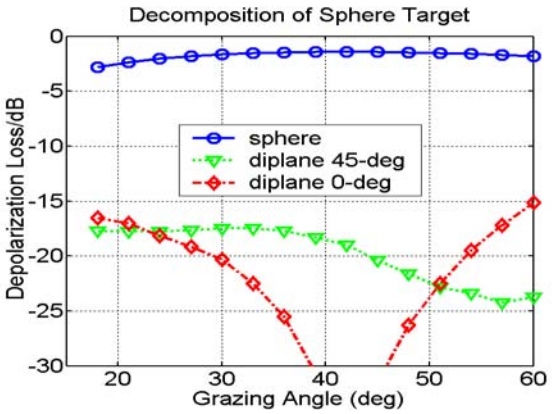

Figure 7. Decomposition of Measured Scatter Matrix from Sphere-like Target

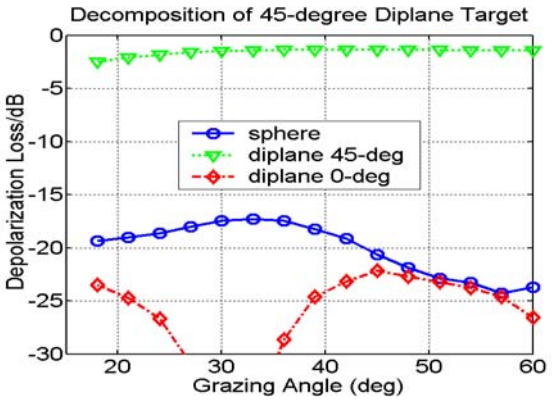

Figure 8. Decomposition of Measured Scatter Matrix from 45-deg Diplane Target

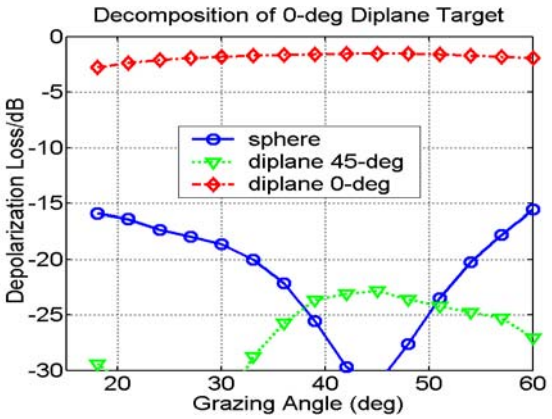

Figure 9. Decomposition of Measured Scatter Matrix from Horizontal (0-deg) Diplane Target

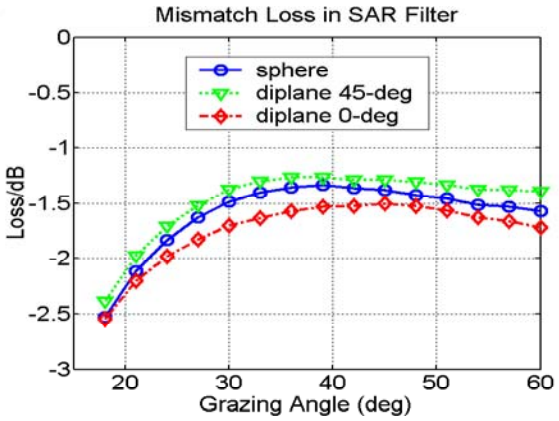

Figure 10. The Mismatch Loss Between the Real Antenna Phase and Amplitude Variation Over Frequency and Angle and the Ideal Variation Postulated in the Weight Matrix, W

6. CONCLUSIONS

A high degree of polarimetric fidelity is achieved among the canonical scatterers, even after being mixed by the polarization response of a practical antenna. Although we cannot draw general conclusions from the performance of a single developmental system, this analysis is an existence proof that compact antennas capable of supporting polarimetric processing of UHF-band UWB SAR and compatible with the constraints of unmanned aircraft can be designed and manufactured. The greatest challenge for antenna designers is at the lowest frequencies, where good cross-polarized rejection is difficult to achieve with size-limited antennas over a wide angular aperture.

Note that for this analysis, we have postulated not only ideal scatterers, but assumed that their scattering matrices are independent of aspect angle. We did this to emphasize antenna effects over inherent geometrical variations within the SAR aperture. Practical SAR polarimetric imagery will include, in addition to antenna depolarization and aspect dependence, additive clutter due both to scatterers within the imaged pixel and to sidelobes of strong scatterers outside the imaged pixel. All these additional effects will further distort the apparent scattering matrices of targets and terrain in the imagery.

REFERENCES

1. Novak, L.M., M.C. Burl, R.D. Cheney, and G.J. Owirka, "Optimal Processing of Polarimetric SAR Imagery," *The Lincoln Laboratory Journal,* v. 3, 1990, p. 273.

2. Cloude, S.R., and E. Pottier, "An Entropy Based Classification Scheme for Land Applications of Polarimetric SAR," *IEEE T–GRS,* 15, 1997, p. 68.

3. Lee, Jong-Sen, M.R. Grunes, and G. DiGrandi, "Polarimetric SAR Speckle Filtering and its Implication for Classification," *IEEE T–GRS,* v. 37, 1999, p. 2363.

4. Novak, L.M., M.C. Burl, and W.W. Irving, "Optimal Polarimetric Processing for Enhanced Target Detection," *IEEE T–AES*, v. 29, 1993, p. 234.

5. Ralston, J.M., and E.L. Ayers, "Full Spatial and Polarimetric Characterization of a UHF Antenna for Ultrawide SAR," *Proc. 2001 IEEE Radar Conf.,* 2001, p. 382.

6. Stutzman, W., *Polarization in Electromagnetic Systems*, Artech House, 1993.

7. Cloude, S.R., K.D. Papathanassiou, and A. Reigber, "Polarimetric SAR Interferometry at P-Band for Vegetation Structure Extraction," *Proc. 3rd European Conf. on Synthetic Aperture Radar (EUSAR 2000),* 2000, p. 249.

REPORT DOCUMENTATION PAGE

Form Approved
OMB No. 0704-0188

Public reporting burden for this collection of information is estimated to average 1 hour per response, including the time for reviewing instructions, searching existing data sources, gathering and maintaining the data needed, and completing and reviewing this collection of information. Send comments regarding this burden estimate or any other aspect of this collection of information, including suggestions for reducing this burden to Department of Defense, Washington Headquarters Services, Directorate for Information Operations and Reports (0704-0188), 1215 Jefferson Davis Highway, Suite 1204, Arlington, VA 22202-4302. Respondents should be aware that notwithstanding any other provision of law, no person shall be subject to any penalty for failing to comply with a collection of information if it does not display a currently valid OMB control number. **PLEASE DO NOT RETURN YOUR FORM TO THE ABOVE ADDRESS.**

1. REPORT DATE	2. REPORT TYPE	3. DATES COVERED *(From–To)*
September 2002	Final	August 2001–July 2002

4. TITLE AND SUBTITLE

Antenna Effects on Polarimetric Imagery in Ultrawide Synthetic Aperture Radar

5a. CONTRACT NUMBER
DAS W01 98 C 0067

5b. GRANT NUMBER

5c. PROGRAM ELEMENT NUMBER

6. AUTHOR(S)
James M. Ralston, Elizabeth Li Ayers

5d. PROJECT NUMBER

5e. TASK NUMBER
DA-2-155

5f. WORK UNIT NUMBER

7. PERFORMING ORGANIZATION NAME(S) AND ADDRESS(ES)

Institute for Defense Analyses
4850 Mark Center Drive
Alexandria, VA 22311-1882

8. PERFORMING ORGANIZATION REPORT NUMBER

IDA Document D-2735

9. SPONSORING / MONITORING AGENCY NAME(S) AND ADDRESS(ES)
DARPA/IXO
3701 N. Fairfax Drive
Arlington, VA 22203

10. SPONSOR/MONITOR'S ACRONYM(S)

11. SPONSOR/MONITOR'S REPORT NUMBER(S)

12. DISTRIBUTION / AVAILABILITY STATEMENT
Approved for public release; distribution unlimited.

13. SUPPLEMENTARY NOTES

14. ABSTRACT

This paper evaluates the effect of practical antenna limitations on the polarimetric quality of ultrawide SAR imagery. For this analysis we have exploited a thorough set of measurements made on a prototype ultrawide SAR antenna designed to meet a set of realistic requirements consistent with use on UAV platforms as well as manned aircraft. These data comprise fully polarimetric, phase-coherent patterns measured over a full 4π steradians. From these data we are able to synthesize the polarimetric response of an ideal target set as it would be measured over an ultrawide SAR aperture (150–550 MHz and 60 deg). By decomposing this synthesized measurement in terms of a canonical basis set of polarized scatterers we can exhibit the level of polarimetric distortions due to a specific practical antenna.

15. SUBJECT TERMS
SAR, foliage penetration, ultra wideband radar, poloarimetry

16. SECURITY CLASSIFICATION OF:			17. LIMITATION OF ABSTRACT	18. NUMBER OF PAGES	19a. NAME OF RESPONSIBLE PERSON
					Lee Moyer
a. REPORT Uncl.	b. ABSTRACT Uncl.	c. THIS PAGE Uncl.	SAR	16	19b. TELEPHONE NUMBER *(include area code)* 703-696-2247

Standard Form 298 (Rev. 8-98)
Prescribed by ANSI Std. Z39.18